INSTITUTE OF PHYSICS PUBLISHING JOURNAL OF PHYSICS: CONDENSED MATTER

J. Phys.: Condens. Matter **15** (2003) 3665–3681 PII: S0953-8984(03)58289-3

Dielectric and magnetic losses of microwave electromagnetic radiation in granular structures with ferromagnetic nanoparticles

L V Lutsev[1], N E Kazantseva[2], I A Tchmutin[2], N G Ryvkina[2], Yu E Kalinin[3] and A V Sitnikoff[3]

[1] Research Institute 'Ferrite-Domen', 8 Chernigovskaya Street, St Petersburg 196084, Russia
[2] Institute of Radio Engineering and Electronics, RAS, 1 Vvedenskii Square, Fryazino, Moscow Region 141190, Russia
[3] Voronezh State Technical University, 14 Moskovsky Prospekt, Voronezh 394026, Russia

Received 14 January 2003, in final form 31 March 2003
Published 23 May 2003
Online at stacks.iop.org/JPhysCM/15/3665

Abstract

We have studied dielectric and magnetic losses in granular structures constituted by ferromagnetic nanoparticles (Co, Fe, B) in an insulating amorphous a-SiO_2 matrix at microwave frequencies, in relation to metal concentration, substrate temperatures and gas content, in the plasma atmosphere in sputtering and annealing. The magnetic losses are due to fast spin relaxation of nanoparticles, which becomes more pronounced with decreasing metal content and occur via simultaneous changes in the granule spin direction and spin polarization of electrons on exchange-split localized states in the matrix (spin-polarized relaxation mechanism). The difference between the experimental values of the imaginary parts of magnetic permeability for granular structures prepared in Ar and Ar + O_2 atmospheres is determined by different electron structures of argon and oxygen impurities in the matrix. To account for large dielectric losses in granular structures, we have developed a model of cluster electron states (CESs). Cluster states are formed by s-electrons of nanoparticles and by electrons in localized states in intergranule regions of the matrix. The observed sharp increase in dielectric losses in the percolation region, the different values of losses for structures sputtered in the Ar and Ar + O_2 atmospheres and reduction of dielectric losses upon annealing, are caused by electric dipole polarization of electrons in CESs.

1. Introduction

Granular structures consisting of ferromagnetic nanoparticles (granules) embedded in an insulating amorphous matrix show interesting microwave properties. Among these are the occurrence of additional modes in the ferromagnetic resonance (FMR) spectrum in a narrow range near the percolation threshold, for which there is no correlation between the wavelength of

spin waves and the film thickness [1–3], sharp increase in the FMR linewidth with decreasing concentration of ferromagnetic nanoparticles [1, 2], and excellent soft magnetic properties governed by the interaction between ferromagnetic granules across intergranular regions [4, 5]. However, the fundamental problem of dielectric and magnetic losses of electromagnetic waves at microwave frequencies in granular structures has not been investigated comprehensively as yet.

In this study, we have analysed experimentally the dielectric and magnetic losses of electromagnetic waves and developed theoretical models explaining the observed dependences. Experiments have been carried out on granular structures of amorphous silicon dioxide with ferromagnetic nanoparticles $Co_{0.4}Fe_{0.4}B_{0.2}$:$(a\text{-}SiO_2)_{100-x}(Co_{0.4}Fe_{0.4}B_{0.2})_x$. We have found that the imaginary parts of the dielectric constant and magnetic permeability, which determine the dielectric and magnetic losses, strongly depend on the metal concentration, substrate temperature reached during the sputtering process, gas content in the plasma atmosphere in sputtering and temperature of annealing after sputtering.

The explanation of the observed dependences of magnetic losses is based on the model developed in [6]. This model describes spin excitations in a single granule with account taken of localized electrons of impurities and defects in the amorphous matrix. The impurities are formed by the reactive gases. These spin excitations are governed by the exchange interaction between d-electrons in a ferromagnetic metal particle and electrons localized on defects and impurities. Relaxation of granule spin excitations and a change in the granule spin direction are accompanied by electron transitions with spin flip between two sublevels of an exchange-split localized states in the matrix. Electron transitions lead to changes in spin polarization of electrons in the localized states. Therefore, this type of relaxation has been named the spin-polarized relaxation (SPR). SPR is rather effective over a wide frequency range. At microwave frequencies, the localized electron states in the matrix, which are magnetically active and have exchange splittings equal to microwave energies, lie far away from the granules. In an ensemble of granules, some exchange splittings are broadened by neighbouring granules and do not contribute to the SPR. This leads to a characteristic feature in the behaviour of SPR at microwave frequencies: with decreasing metal particle concentration, the number of localized states, with exchange splitting of the order of the microwave energy per granule, grows, and the SPR decay constant therefore becomes higher. We use the spin Green function of a single granule to obtain a relation between the spin relaxation decay constant of a granule and the imaginary part of the magnetic permeability of the granular structure. We solve the inverse problem, i.e. find the decay constant of the granule spin relaxation, from the experimental data on the imaginary part of the magnetic permeability. The spin relaxation is of the SPR type, and the observed magnetic losses are therefore determined by the SPR mechanism.

The experiment shows a sharp increase in the imaginary part of the dielectric constant in the percolation region. Using transmission electron microscopy (TEM), we have observed that there are no direct contacts between granules. Nevertheless, strong dipoles appear in the granular structure in the percolation region. We explain the observed sharp increase in dielectric losses with increasing metal content in the percolation region and the reduction of losses upon annealing in terms of the model of cluster electron states (CESs) in granular structures [7]. CESs are formed by s-electrons of granule clusters (groups of particles) near the Fermi level and by electrons of localized states in intergranule regions of the matrix. The presence of CESs gives rise to localized conducting clusters with large dipole momenta. Above the percolation threshold, CESs form a network of an infinite conducting cluster. The characteristic localization size of CESs is determined by localization of s-electrons, which depends on the distribution of depths of potential wells formed by metal granules, on the coefficient of electron tunnelling between granules and on the density of impurities in the intergranule regions. If

the average CES localization size is large, the electric dipole polarization of CESs leads to a high dielectric constant of the granular structure. We have found the imaginary part of the dielectric constant in the random phase approximation (RPA) for a diagram expansion of the CES Green function.

2. Experiment

The experiments were performed on samples of amorphous silicon dioxide containing nanosize inclusions of a ferromagnetic alloy, designated as $(\text{a-SiO}_2)_{100-x}(\text{Co}_{0.4}\text{Fe}_{0.4}\text{B}_{0.2})_x$. The $(\text{a-SiO}_2)_{100-x}(\text{Co}_{0.4}\text{Fe}_{0.4}\text{B}_{0.2})_x$ films were grown on corundum-based ceramic substrates by ion–plasma co-sputtering of silicon dioxide and ferromagnetic alloy $\text{Co}_{0.4}\text{Fe}_{0.4}\text{B}_{0.2}$ targets in argon and argon–oxygen plasmas. The concentration of metal nanoparticles in the silicon dioxide deposit was varied by changing the ratio of alloy and a-SiO_2 target areas. The films were deposited onto cold substrates ($T = 20\,^{\circ}\text{C}$) and those heated to 250 °C. The film thicknesses are in the range 10–16 μm. The film composition was determined by x-ray microanalysis and TEM. For the samples studied, the relative content of metal x varies from 22.4 to 71 at.%. The average size of metal particles increases with x: from 2.0 nm at $x = 22.4$ at.% to 5 nm at $x = 71$ at.%. Metal nanoparticles are in the ferromagnetic state.

The imaginary parts of the dielectric constant and the magnetic permeability were determined by the resonance–waveguide method with R2-series network analysers in the frequency range 4.8–16.6 GHz. Experiments were carried out at fixed frequencies of 4.8, 6.6, 11.1 and 16.6 GHz. We used $0.5 \times 1 \times 50$ mm samples to measure the imaginary part of the dielectric constant and 0.5 mm $\times$ 2 mm $\times$ 50 mm samples to measure the imaginary part of the magnetic permeability. Using the resonance–waveguide method, we eliminated the substrate influence and determined the dielectric and magnetic characteristics of granular films. Experiments were carried out at low applied microwave power (2–5 mW). This rules out sample heating during measurements. The dielectric and magnetic characteristics of the granular films were measured with accuracy of 10–15%. Experiments were carried out on as-sputtered and annealed granular films. Annealing was done for 30 min at temperatures 400 and 450 °C in a vacuum better than 100 μTorr. Figure 1 shows the imaginary part of the magnetic permeability, μ'', versus the metal concentration x for as-sputtered and annealed granular structures at a frequency of 4.8 GHz. Films sputtered in the Ar atmosphere exhibit high values of μ'' (figure 1(a)). The magnitude of μ'' grows with increasing concentration of ferromagnetic nanoparticles. Annealing makes the magnetic permeability lower. By contrast, granular structures prepared in the argon–oxygen atmosphere (4–4.5 at.% O_2) show lower values of μ'' (figures 1(b) and (c)). Annealing makes these values higher. For granular films sputtered onto cold substrates (at $T = 20\,^{\circ}\text{C}$), the μ'' dependence shows a maximum at metal concentration $x = 53$ at.% (figure 1(b)). This feature is not observed for granular structures deposited onto substrates heated to 250 °C. Frequency dependences of μ'' are presented in figure 2 for granular structures deposited in $\text{Ar} + \text{O}_2$ atmosphere onto cold ($T = 20\,^{\circ}\text{C}$) substrates. It can be seen that the imaginary part of the magnetic permeability passes through a maximum in the frequency range 6–8 GHz.

Figure 3 shows the imaginary part of the dielectric permittivity, ε'', versus the metal concentration x. It can be seen that granular structures sputtered in the Ar plasma have greater values of ε'' than structures prepared in $\text{Ar} + \text{O}_2$. Granular films deposited onto cold substrates in the $\text{Ar} + \text{O}_2$ plasma have maximum ε'' at metal concentration of 55 at.% (figure 3(b)). Annealing makes the dielectric constant lower. Typical frequency dependences of ε'' are presented in figure 4. The main tendency exhibited by these curves is that ε'' decreases with increasing frequency.

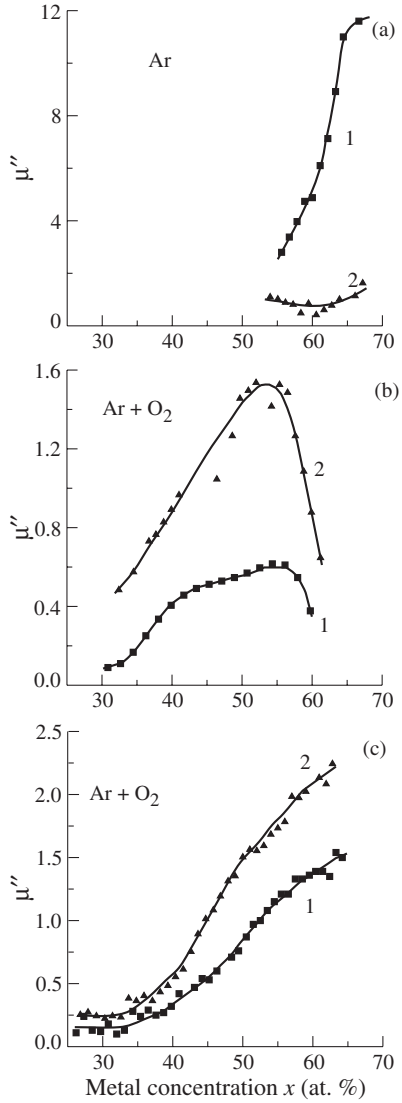

Figure 1. Imaginary part of the magnetic permeability, μ'', of granular structures $(\text{a-SiO}_2)_{100-x}(\text{Co}_{0.4}\text{Fe}_{0.4}\text{B}_{0.2})_x$ versus the metal concentration x at a frequency of 4.8 GHz. (a) Structures deposited onto substrates heated to 250 °C in Ar plasma; 1, as-sputtered; 2, annealed at 400 °C. (b) Structures deposited onto substrates cooled to 20 °C in Ar + O_2 plasma (4 at.% O_2): 1, as-sputtered; 2, annealed at 450 °C. (c) Structures deposited onto substrates heated to 250 °C in Ar + O_2 plasma (4.5 at.% O_2): 1, as-sputtered; 2, annealed at 400 °C.

Figure 5 shows the concentration dependences of the electrical resistivity ρ of $(\text{a-SiO}_2)_{100-x}(\text{Co}_{0.4}\text{Fe}_{0.4}\text{B}_{0.2})_x$ granular films, measured at room temperature on samples in the original state and after annealing. After the heat treatment, the concentration dependences of the electrical resistivity assumed an S-shaped form characteristic of percolation systems. Annealing of granular structures results in an increase in the electrical resistivity for compositions with low concentration of the metal phase and its decrease for large x. The S-shaped resistivity curve obtained for annealed samples suggests that annealed granular

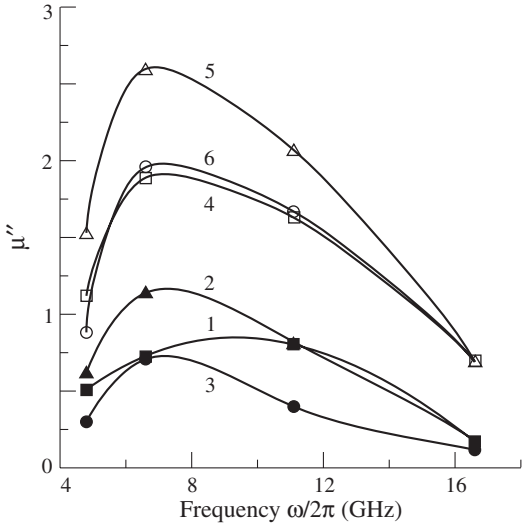

Figure 2. Frequency dependence of the imaginary part of magnetic permeability, μ'', of granular structures $(\text{a-SiO}_2)_{100-x}(\text{Co}_{0.4}\text{Fe}_{0.4}\text{B}_{0.2})_x$ deposited onto substrates cooled to 20 °C in $\text{Ar} + \text{O}_2$ plasma (4 at.% O_2): 1, $x = 45$ at.% as-sputtered; 2, $x = 55$ at.% as-sputtered; 3, $x = 60$ at.% as-sputtered; 4, $x = 45$ at.% annealed at 450 °C; 5, $x = 55$ at.% annealed at 450 °C; 6, $x = 60$ at.% annealed at 450 °C.

structures approach the termite limit with metal resistivity $\rho_{\text{me}} = 0$ [8, 9]. The percolation region has been determined from a change in the behaviour of the temperature dependences of the resistivity ρ, more specifically, from a transition from the non-metallic type of resistivity to the metallic type. This region lies approximately at metal concentrations of 52–58 at.% [10, 11]. This concentration range coincides with that in which the maximum slope of the resistivity curves is observed in figure 5. In the percolation region, spins of metal nanoparticles are strongly correlated due to tunnelling electrons. Below this region, weak magnetic dipolar interactions are dominant and the magnetic ordering disappears at room temperature [12]. The granular structure is in the superparamagnetic state.

3. Magnetic losses

To explain the observed features of magnetic loss dependences below the percolation region we find the magnetic permeability of granular structures in the superparamagnetic state, consider the SPR and solve the inverse problem, i.e. calculate the decay constant of the granule spin relaxation from the experimental data on the imaginary part of the magnetic permeability. The SPR mechanism of relaxation allows us to explain the influence of reactive gases and annealing.

3.1. Spin-polarized relaxation and magnetic permeability

Let us consider an ensemble of ferromagnetic granules and unpaired localized electrons of impurities and defects in the amorphous matrix. The localized electron states in the matrix are related to defects of the matrix and to impurities formed by the reactive gases. We assume that below the percolation region magnetic correlations between granules disappear and magnetic dipolar interactions are too weak to produce spin ordering in the ensemble of

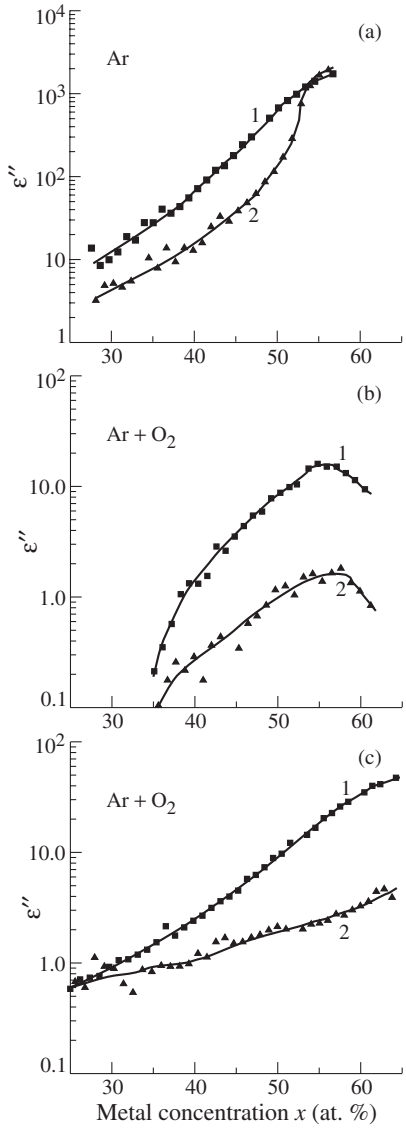

Figure 3. Imaginary part of dielectric constant, ε'', of granular structures $(\text{a-SiO}_2)_{100-x}(\text{Co}_{0.4}\text{Fe}_{0.4}\text{B}_{0.2})_x$ versus the metal concentration x at a frequency of 4.8 GHz. (a) Structures deposited onto substrates heated to 250 °C in Ar plasma: 1, as-sputtered; 2, annealed at 400 °C. (b) Structures deposited onto substrates cooled to 20 °C in Ar + O_2 plasma (4 at.% O_2): 1, as-sputtered; 2, annealed at 450 °C. (c) Structures deposited onto substrates heated to 250 °C in Ar + O_2 plasma (4.5 at.% O_2): 1, as-sputtered; 2, annealed at 400 °C.

granules. Therefore, the granule spins have random directions, i.e. the granular structure is in the superparamagnetic state. To obtain the magnetic permeability of the granular structure we must know spin excitations and the spin Green function of a single granule. The spin excitations in a single granule have been studied [6] in the framework of the s–d-exchange model in the one-loop approximation with respect to the s–d-exchange interaction for a diagram expansion of the spin Green function. The diagram expansion is based on the diagram technique

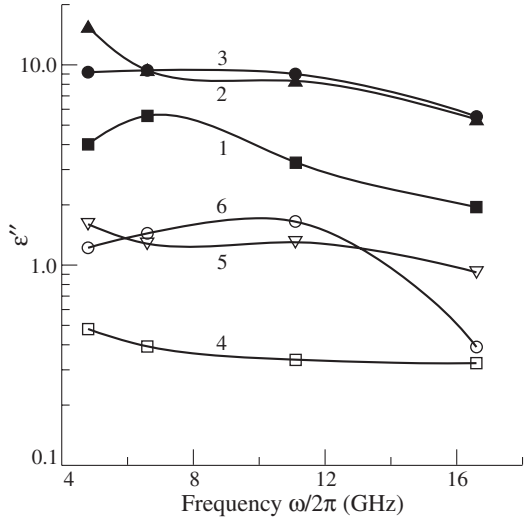

Figure 4. Frequency dependence of the imaginary part of dielectric constant, ε'', of the granular structures $(\text{a-SiO}_2)_{100-x}(\text{Co}_{0.4}\text{Fe}_{0.4}\text{B}_{0.2})_x$ deposited onto substrates cooled to 20 °C in $\text{Ar} + \text{O}_2$ plasma (4 at.% O_2): 1, $x = 45$ at.% as-sputtered; 2, $x = 55$ at.% as-sputtered; 3, $x = 60$ at.% as-sputtered; 4, $x = 45$ at.% annealed at 450 °C; 5, $x = 55$ at.% annealed at 450 °C; 6, $x = 60$ at.% annealed at 450 °C.

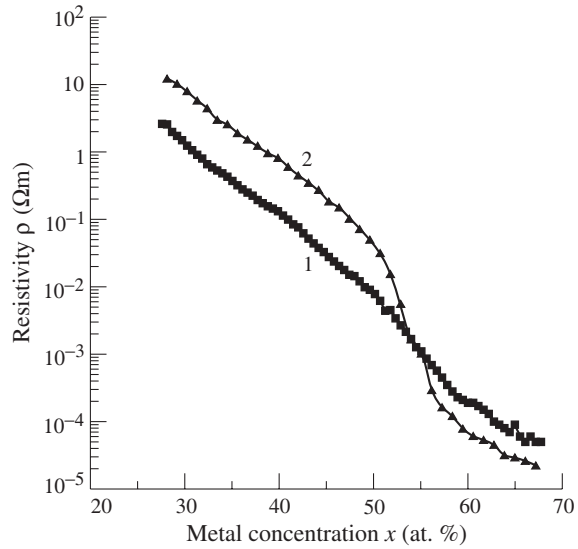

Figure 5. Electrical resistivity ρ of granular structures $(\text{a-SiO}_2)_{100-x}(\text{Co}_{0.4}\text{Fe}_{0.4}\text{B}_{0.2})_x$ versus the metal concentration x: 1, as-sputtered; 2, annealed at 400 °C.

for spin operators [13]. The d-system is represented by d-electron spins of the granule. Unpaired localized electrons of impurities and defects in the amorphous matrix constitute the s-system. The s- and d-systems are coupled through the exchange interaction $J(r)$. The spin excitations of a single granule are determined by poles of the transverse spin Green function $K^{\mp\pm}(\omega)$. The transverse spin Green function of the granule is equal to the Fourier

transform of temperature spin Green function $\langle\langle \tilde{S}^{\mp}\tilde{S}^{\pm}(\omega_n)\rangle\rangle_0$ with analytical continuation $i\omega_n \to \omega + i\epsilon \mathrm{sign}\omega (\epsilon \to +0)$ [6]

$$K^{\mp\pm}(\omega) = \langle\langle \tilde{S}^{\mp}\tilde{S}^{\pm}(\omega_n)\rangle\rangle_0|_{i\omega_n\to\omega+i\epsilon\mathrm{sign}\omega} = \frac{2\langle S\rangle_0}{\beta\hbar(\Omega - i\delta \mp \omega)} \tag{1}$$

where $\tilde{S}^{\pm}$ is the spin operator of the d-electrons in the Heisenberg representation, $\Omega = g\mu_B H/\hbar$, $\beta = 1/kT$, k is the Boltzmann constant, T is temperature, ω is the frequency of the ac magnetic field $\boldsymbol{h}$ exciting the granule spins, δ is the decay constant or the inverse relaxation time of the granule spin excitation, g is the Landé factor, μ_B is the Bohr magneton, and $\langle S\rangle_0$ is the statistical-average d-electron spin whose direction is parallel to the internal field $\boldsymbol{H}$. $\boldsymbol{H}$ is the self-consistent field acting on the granule, which is equal to the sum of the magnetic field of neighbouring ferromagnetic granules, the depolarizing magnetic field originating from the granule shape and the field determined by the exchange interaction J.

The decay constant δ is determined by the SPR. According to the SPR mechanism, the change in the granule spin direction is accompanied by an electron transition between two sublevels of an exchange-split localized state in the matrix. The electron transition leads to a change in the spin polarization of this localized electron in the matrix. Owing to spin–orbit coupling, excitations of electrons on localized states turn into phonon excitations in the matrix. If the spacing Δ between the Fermi level in a metal particle and the bottom mobility edge of the conduction band in the matrix is greater than kT (figure 6(a)), the SPR decay constant of spin excitations in the granule to a first order in the reciprocal radius of the exchange interaction is given by [6]

$$\delta(\omega) = \frac{2\pi^2\bar{g}\omega(\hbar\omega - g\mu_B H)}{\xi^3\langle S\rangle_0}\ln^2\frac{2J_0\langle S\rangle_0}{\hbar\omega - g\mu_B H} \tag{2}$$

where $\bar{g}$ is the density of localized states in the matrix near the Fermi level, $J(R) = J_0\exp(-\xi R)$, R is the distance from the centre of the localized state to the granule boundary, and ξ is the reciprocal radius of the exchange interaction.

At microwave frequencies and $\langle S\rangle_0 \gg 1$, the exchange-split levels of localized electron states in the matrix, which are involved in the SPR, have exchange splittings equal to the microwave energy $\hbar\omega$ [6] and lie at a greater distance from granule boundaries compared with the radius of the exchange interaction: $R = \xi^{-1}\ln(J_0\langle S\rangle_0/\hbar\omega)$ (figure 6(a)). For $J_0 = 0.01$ eV, $\langle S\rangle_0 = 10$, $\omega/2\pi = 10$ GHz, the distance R is $30.8\xi^{-1}$. In figures 6(b) and (c), these levels, which determine the spin relaxation of the granule A, are at a distance R from the granule A and cannot lie at a distance shorter than R from neighbouring granules. With increasing granule concentration x, these energy exchange splittings are broadened by neighbouring granules and give no contribution to the SPR at a given ω. This decreases the number of magnetically active matrix levels per granule. Therefore, the SPR decay constant δ decreases with increasing metal content.

The magnetic permeability tensor μ_{ij} is found by summation of the spin Green functions K^{ij} ($i, j = \{x, y, z\}$) over all granules N in the volume V of the granular structure

$$\mu_{ij}(\omega) = 1 + \frac{4\pi\beta(g\mu_B)^2}{V}\sum_{n=1}^{N} K^{(n)ij}(\omega)\sin\theta_i^{(n)}\sin\theta_j^{(n)} \tag{3}$$

where $\theta_i^{(n)}$, $\theta_j^{(n)}$ are the angles between the direction of spin of the nth granule and the axes i, j, respectively. We assume that

(a) $\theta_i^{(n)}$ is a random variable in the range $[0, \pi]$;

(b) there is no correlation between $\theta_i^{(n)}$ and the self-consistent field $\boldsymbol{H}^{(n)}$ acting on the nth granule;

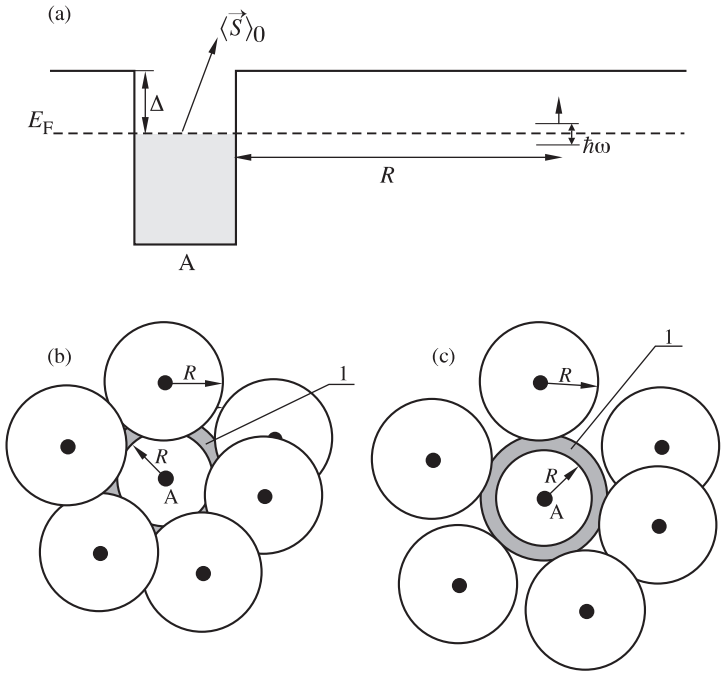

Figure 6. (a) Energy structure of granule A and unpaired electron on localized state with exchange splitting equal to the microwave energy $\hbar\omega$. The change in the granule spin leads to an electron transition and to a change in the spin polarization of the electron on the localized state. Areas of matrix localized electron states with microwave energy spacing (1), which are magnetically active in spin relaxation of granule A according to the SPR model for (b) high and (c) low granule concentrations. R is the distance from a granule to active localized electron states.

(c) there is no correlation between the angles $\theta_i^{(n)}$, $\theta_j^{(m)}$ of neighbouring granules n, m;
(d) the characteristic time of fluctuations of the self-consistent field direction is large in comparison with ω^{-1};
(e) the self-consistent field H is a random variable with distribution $f(\Omega) = f(g\mu_B H/\hbar)$.

Then, taking into account that summation of squared sines of the random variables over all granules gives $N^{-1}\sum_n \sin^2\theta_i^{(n)} = 1/2$, we obtain that the tensor μ_{ij} in equation (3) has only diagonal components $\mu = \mu_{ii}$, which are determined by the transverse Green functions $K^{(n)-+}$, $K^{(n)+-}$ (see equation (1)). The assumptions made above allow us to write μ in the form

$$\mu(\omega) = 1 + \frac{\pi\beta(g\mu_B)^2}{2V}\sum_{n=1}^{N}[K^{(n)-+}(\omega) + K^{(n)+-}(\omega)] = 1 + \frac{p\Omega_M}{2}\int_0^\infty \frac{f(\Omega)(\Omega - i\delta)}{(\Omega - i\delta)^2 - \omega^2}\,d\Omega \tag{4}$$

where $\Omega_M = 4\pi(g\mu_B)^2\langle S\rangle_0/\hbar v_g = 4\pi g\mu_B M/\hbar$; $M = g\mu_B\langle S\rangle_0/v_g$ is the granule magnetization; p is the relative granule volume, which can be written as

$$p = \frac{x v_g}{x v_g + (100 - x)v_m}. \tag{5}$$

$v_g = m_g/\rho_g N_A$, $v_m = m_m/\rho_m N_A$ are atomic volumes for the granule and matrix; m_g, m_m are the respective atomic masses; ρ_g, ρ_m are the densities of granules and the matrix; N_A is

the Avogadro number; x is the granule concentration. The imaginary part of the magnetic permeability is given by

$$\mu''(\omega) = \frac{p\Omega_M\delta}{2}\int_0^\infty \frac{f(\Omega)(\Omega^2+\delta^2+\omega^2)}{(\Omega^2-\delta^2-\omega^2)^2+4\Omega^2\delta^2}\,\mathrm{d}\Omega. \tag{6}$$

3.2. Inverse problem. Spin-relaxation decay constant of granules

Relation (6) can be considered an integral equation in the function $f(\Omega)$ and decay constant δ depending on the parameter ω. We assume that $f(\Omega)$ can be approximated by the normal distribution with variance σ and mean value $\Omega_0 = g\mu_B H_0/\hbar$, determined by the average self-consistent internal field H_0

$$f(\Omega) = \frac{1}{(2\pi)^{1/2}\sigma}\exp\left[\frac{-(\Omega-\Omega_0)^2}{2\sigma^2}\right]. \tag{7}$$

Taking into account relation (7) and known values of $\mu''(\omega)$ in the investigated frequency range, we can convert integral equation (6) into a set of equations in the unknown variables δ, σ, H_0 and can solve the inverse problem to find δ, σ and H_0. To obtain the decay constant from experimental data, we assume that, to a first approximation, the decay δ is independent of the frequency ω in the frequency range considered (4.8–16.6 GHz), and $\sigma \ll \delta$. Then, neglecting higher orders of σ/δ, we find the solution to equation (6), which depends on two variables $\bar{\delta}$ and Ω_0, where $\bar{\delta} = \delta + (2\ln 2)^{1/2}\sigma$ is the generalized decay constant. Figure 7 shows $\bar{\delta}$ as a function of the granule concentration x in the granular structure $(\text{a-SiO}_2)_{100-x}(\text{Co}_{0.4}\text{Fe}_{0.4}\text{B}_{0.2})_x$, calculated from equation (6). The decay constants $\bar{\delta}$ for granular structures prepared in the Ar + O_2 plasma increase with decreasing granule concentration at $x < 40$ at.% in figure 7(b) and at $x < 50$ at.% in figure 7(c). This increase in the $\bar{\delta}$ decay below the percolation region is in agreement with the SPR mechanism of granule spin relaxation, expressed by equation (2). This behaviour of $\bar{\delta}$ cannot be governed by σ. The variance of the self-consistent internal field σ cannot grow with decreasing x, because the mean value and the variance of the magnetic field of neighbouring ferromagnetic granules falls with decreasing x and, on the average, the depolarizing magnetic field originating from the granule shape does not vary: relative shapes of granules undergo no changes. Therefore, the decay δ makes a major contribution to $\bar{\delta}$, and the assumption that $\sigma \ll \delta$ is correct. The fact that the magnetic loss grows with decreasing granule concentration leads us to conclude that the observed magnetic losses are due to the SPR.

The localized electron states in the matrix are related to defects of the amorphous matrix and to impurities formed by the reactive gases. As-sputtered films prepared in the Ar atmosphere (figure 7(a)) are characterized by lower magnetic losses than films deposited in the Ar + O_2 atmosphere (figures 7(b) and (c)). This is due to different electronic structures of gas impurities in the a-SiO_2 matrix. Argon atoms have filled the outer electron shell. In the matrix, argon atoms form impurities with filled exchange-split levels. Electron transitions between filled sublevels of these exchange-split localized states cannot occur, and the localized states are not polarized. Impurities of this kind take no part in the SPR. Annealing may remove some electrons from the filled shells of these impurities, so that the impurity becomes polarizable. This leads to an increase in magnetic losses (figure 7(a)). In contrast to argon atoms, oxygen atoms have an incomplete outer electron shell. Oxygens form in the matrix impurities with partially filled exchange-split levels. Impurities with incomplete exchange levels are magnetically active and can be polarized. They take part in the SPR. Annealing partly eliminates defects and, therefore, matrix localized states. This decrease may reduce somewhat the magnetic losses (figures 7(b) and (c)).

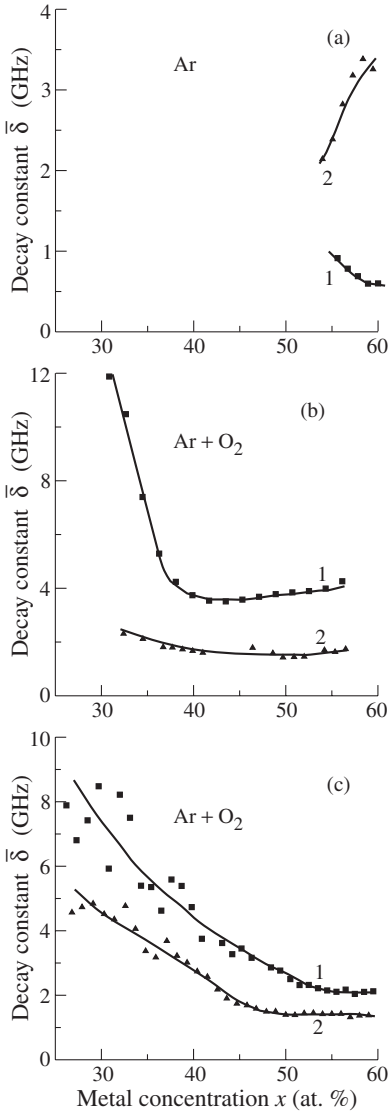

Figure 7. Decay constant $\bar{\delta}$ of spin excitations in granular structures $(a\text{-}SiO_2)_{100-x}(Co_{0.4}Fe_{0.4}B_{0.2})_x$ versus the metal concentration x in the frequency range 4.8–16.6 GHz. (a) Structures deposited onto substrates heated to 250 °C in Ar plasma: 1, as-sputtered, 2, annealed at 400 °C. (b) Structures deposited onto substrates cooled to 20 °C in Ar + O_2 plasma (4 at.% O_2): 1, as-sputtered; 2, annealed at 450 °C. (c) Structures deposited onto substrates heated to 250 °C in Ar + O_2 plasma (4.5 at.% O_2): 1, as-sputtered; 2, annealed at 400 °C.

If granular films are sputtered onto cold substrates in the Ar + O_2 plasma, the imaginary part of the magnetic permeability has the maximum value at $x = 53$ at.% (figure 1(b)). This may be due to the appearance of correlations between spin directions of neighbouring granules in the percolation region. The low substrate temperature favours freezing of spin correlations. In this case, relation (4), proved for the superparamagnetic phase, is incorrect for the percolation region because the angles $\theta_i^{(n)}$ in equation (3) are not random variables. The spin correlations

may reduce the magnetic permeability. This assumption requires additional experiments and we are going to verify it in the next study.

Solution of equation (6) gives not only the decay constant, but also the mean value Ω_0, which is related to the average self-consistent internal field H_0. We have obtained that the internal field ranges from 1900 to 2800 Oe in the metal concentration range 22.4–60 at.%. These values correspond to the maximum in the frequency dependence of the imaginary part $\mu''(\omega)$ in figure 2.

4. Dielectric losses

An increase in dielectric losses with increasing metal content is observed in the percolation region for the granular structures studied (figure 3). In the percolation region (55–60 at.%) for granular structures prepared in Ar plasma, the imaginary parts of the dielectric constant, ε'', are 200–300 times the values of ε'' for structures with metal concentrations 25–35 at.%. For as-sputtered structures prepared in the $Ar + O_2$ atmosphere, the dielectric losses increase by a factor of 40–70. Annealing reduces the dielectric constant. TEM shows that there are no direct contacts between granules. Nevertheless, strong dipoles appear in the granular structure in the percolation region. The classical theoretical model of percolation cannot account for these facts. According to the classical model, conducting clusters are formed in a granular structure from metal particles whose boundaries are in contact with one another [8–14]. The polarization of conducting clusters determines the dielectric constant [15]. Tunnelling between granules, defects and localized electron states in the matrix is disregarded by the classical model of percolation. The observed growth of the average size of metal nanoparticles cannot also account for the increase in dielectric losses. We take into account the tunnelling and localized states in the matrix and develop a model of the dielectric constant, based on CESs. This model can account for the observed influence of annealing and reactive plasma gases on the dielectric constant of granular structures.

4.1. Cluster electron states

Let us consider an electron near the Fermi level in a metal granule. If tunnelling between granules takes place, then this electron in the granule can be localized on a group (cluster) of granules [16]. The wavefunction Ψ_α of this state, which is called the CES [7], is formed by the sum of wavefunctions $\psi_\lambda^{(n)}$ of s-electrons in granules and wavefunctions $\varphi_\nu^{(i)}$ of localized states in intergranule regions

$$\Psi_\alpha(\boldsymbol{r}) = \sum_{n,\lambda} a_{\alpha\lambda}^{(n)} \psi_\lambda^{(n)}(\boldsymbol{r}) + \sum_{i,\nu} b_{\alpha\nu}^{(i)} \varphi_\nu^{(i)}(\boldsymbol{r}) \tag{8}$$

where α, λ, ν are indices of eigenvalues for CESs, s-electrons in the granule and localized states in the matrix, respectively; $a_{\alpha\lambda}^{(n)}$, $b_{\alpha\nu}^{(i)}$ are factors. The summation is performed over the index n of granules, index i of localized states and indices of eigenvalues λ, ν. The characteristic CES localization size depends on the distribution of depths of potential wells formed by granules, on the coefficient of electron tunnelling between granules, and on the density of impurities in intergranule regions.

In the case when the granule size d plays the role of the random parameter, the CES localization can be described in terms of the Anderson localization model [7, 17]. The random distribution of d leads to a random variation of the granule capacitance C and the potential well depth in granules, which is given by the Coulomb energy shift induced by an electron present in the granule (figure 8(a)). The CES localization size L is determined by the electron tunnelling

coefficient I and by the scatter of well depths $V_0 = \max_n(e^2/2C^{(n)}) - \min_n(e^2/2C^{(n)}) = 2e^2\Delta d/\bar{\varepsilon}(d_0^2 - \Delta d^2)$, where Δd is the scatter of granule dimensions d; d_0 is the average granule size; $\bar{\varepsilon}$ is the dielectric constant of the matrix; n is the index denoting granules contained in the CES group of nanoparticles. To a first Born approximation [7]

$$L = 16\pi d_0 p^{-4/3}\left(\frac{I}{V_0}\right)^2 \tag{9}$$

where the relative granule volume p is given by relation (5). The electron tunnelling coefficient $I \propto \exp(-\eta l)$ appearing in (9) depends on the distance l between neighbouring granules and the transparency coefficient η, which is a functional of the wavefunctions $\varphi_\nu^{(i)}$ of localized states in the matrix in relation (8) and of the barrier height. If the granule concentration $x \to 0$, the CES localization size L approaches zero. For granule concentrations x below the percolation threshold the CES size grows with increasing x in accordance with

$$L \propto x^{-4/3}\exp\left[-\eta d_0\left(\frac{v_m}{v_g}\right)^{1/3}\left(\frac{x}{100}\right)^{-1/3}\right]. \tag{10}$$

The phonon-induced inelastic resonance electron tunnelling via a chain of localized states in the matrix leads to a sharp increase in the transparency of the tunnelling barrier [18, 19]. In this case, the CES size L increases considerably. Annealing makes the number of defects and localized states in the matrix smaller. This leads to a decrease in the tunnelling transparency, manifested as a decrease in the conductivity of granular structures below the percolation threshold [20]. In this case, the CES localization size becomes smaller.

The CES energy levels are shifted to below the Fermi level (figure 8(a)). The whole set of localized CES levels can be regarded as a predecessor of the metal conduction band. In the percolation region, the CES localization size L increases, and, above the percolation threshold, CESs form an infinite conducting cluster network. At high granule concentrations, when the granular structure is close to a metal, the set of CES levels turns into the conduction band.

4.2. Dielectric constant

Electrons in CESs can be polarized by an electric field. CESs have electric dipole momenta exceeding those of granule dipoles (figure 8(b)). Polarization of electric dipoles of CESs determines the dielectric constant ε of the granular structure. To obtain ε, we use the temperature Green function diagram technique. In the RPA approximation, the dielectric constant is given by (figure 8(c)) [21]

$$\begin{aligned}\varepsilon(\boldsymbol{q},\omega) &= 1 - (-1)^m\beta V(\boldsymbol{q})\sum_{\substack{\sigma,\tau,\omega_l\\ \sigma\neq\tau}}|M_{\sigma\tau}(\boldsymbol{q})|^2 G_\sigma(\omega_l)G_\tau(\omega_n+\omega_l)\Big|_{\mathrm{i}\omega_n\to\omega+\mathrm{i}\gamma\,\mathrm{sign}\,\omega}\\ &= 1 + V(\boldsymbol{q})\sum_{\substack{\sigma,\tau\\ \sigma\neq\tau}}\frac{|M_{\sigma\tau}(\boldsymbol{q})|^2[n_\mathrm{F}(\beta E_\sigma) - n_\mathrm{F}(\beta E_\tau)]}{\mathrm{i}\hbar\omega_n - E_\tau + E_\sigma}\Big|_{\mathrm{i}\omega_n\to\omega+\mathrm{i}\gamma\,\mathrm{sign}\,\omega}\end{aligned} \tag{11}$$

where $m = 1$ is the number of fermion loops; $V(\boldsymbol{q})$ is the Fourier transform of the Coulomb interaction e^2/r of electrons placed on CES groups;

$$G_\sigma(\omega_n) = \frac{1}{\beta(\mathrm{i}\hbar\omega_n - E_\sigma)}$$

is the temperature Green function of the CES Ψ_σ with the energy level E_σ; $\beta\hbar\omega_n = 2(n+1)\pi$; $\gamma \to +0$;

$$M_{\sigma\tau}(\boldsymbol{q}) = \int \Psi_\sigma^*(\boldsymbol{r})\exp(-\mathrm{i}\boldsymbol{q}\boldsymbol{r})\Psi_\tau(\boldsymbol{r})\,\mathrm{d}\boldsymbol{r}$$

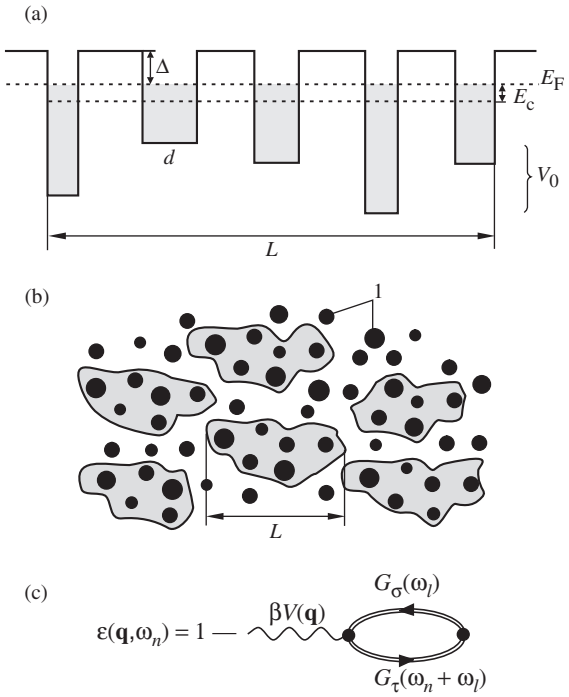

Figure 8. (a) Energy structure of a CES. Random distribution of depths V_0 of potential wells in a granule are determined by random variation of granule capacitances. L is the CES localization size. (b) CES in a granular structure: 1, granules. (c) RPA approximation diagram for the dielectric constant determined by the CES dipole polarization.

is the vertex factor represented by the matrix element of the transition between CESs σ and τ; $\boldsymbol{q}$ is the wavevector of the applied electrical field; $n_F(x) = [\exp(x) + 1]^{-1}$.

To calculate the imaginary part of the dielectric constant, ε'', we assume that

(a) the wavefunction $\Psi_\alpha(\boldsymbol{r})$ (8) has the form

$$\Psi_\alpha(\boldsymbol{r}) = \Psi_{Q_n}(\boldsymbol{r}) = L^{-3/2}\exp(\mathrm{i}\boldsymbol{Q_n r})$$

where the index $\alpha = (Q_{n_x}, Q_{n_y}, Q_{n_z})$, $\boldsymbol{Q_n} = 2\pi(n_x \boldsymbol{i_x} + n_y \mathrm{i}_y + n_z \mathrm{i}_z)/L$, $n_x, n_y, n_z = 0, 1, 2, \ldots$;

(b) the energy spectrum of CESs, E_σ, is analogous to the spectrum of a particle with effective mass m^* in a well of depth E_c and width L (figure 8(a))

$$E_\sigma = E_{Q_n} = \frac{\hbar^2|\boldsymbol{Q_n}|^2}{2m^*} - E_c;$$

(c) the wavevector $\boldsymbol{q}$ of the applied electrical field is smaller than $\boldsymbol{Q_n}$: $|\boldsymbol{q}| \ll |\boldsymbol{Q_n}|$;

(d) the frequency ω of the applied field is much smaller than $kT/\hbar$ and $E_c/\hbar$: $\hbar\omega \ll kT$, $\hbar\omega \ll E_c$;

(e) the spacing Δ between the Fermi level of a metal particle and the bottom mobility edge of the conduction band in the matrix is large in comparison with kT: $\Delta \gg kT$.

If these assumptions are valid, then, to a first approximation in $|\boldsymbol{q}|/|\boldsymbol{Q_n}|$, $|\boldsymbol{q}|/|\boldsymbol{Q_l}|$, the matrix element of the transition between CES levels, determined by $\boldsymbol{Q_n}$ and $\boldsymbol{Q_l}$, can be written

in the form

$$M_{Q_n Q_l}(\boldsymbol{q}) = \frac{(-1)^{n_x - l_x}|\boldsymbol{q}|\delta_{n_y l_y}\delta_{n_z l_z}}{Q_{n_x} - Q_{l_x}} \tag{12}$$

where $\boldsymbol{q} \parallel x$ and $n_x \neq l_x$.

Taking into account relations (11) and (12), using the formula $(x - \mathrm{i}0)^{-1} = \mathcal{P}1/x + \mathrm{i}\pi\delta(x)$, and disregarding the discrete nature of the energy spectrum of CESs, which can be done at $kT \gg 2\pi^2\hbar^2/m^*L^2$, we obtain the imaginary part of the dielectric constant

$$\varepsilon''(\boldsymbol{q}, \omega) = \frac{e^2 m^* L k T}{\pi\hbar^3\omega} \ln\left[1 + \exp\left(\frac{E_c}{kT}\right)\right]. \tag{13}$$

If $kT < 2\pi^2\hbar^2/m^*L^2$, then the exponential term in equation (13) must be dropped and ε'' decreases linearly as the temperature is lowered.

Using relation (13), we can explain the observed sharp increase in ε'' in the percolation region (figure 3). Raising the metal concentration x leads to a sharp increase in the transparency of the tunnelling barrier at the percolation threshold. According to equation (9) and proportion (10), this is why the CESs substantially grow in size L. Electron polarization on CESs determines the dielectric constant. Large L and high energy E_c in equation (13) in the percolation region give high values of ε''.

The transparency coefficient η of the tunnelling barrier in (10) strongly depends on the number of localized states in the matrix between granules and on the thickness of the oxide granule boundary layer. The presence of oxide boundaries is the most probable reason for the decrease in ε'' in granular structures sputtered in the Ar + O_2 atmosphere in comparison with granular structures sputtered in the Ar plasma.

Annealing makes the number of defects and localized electron states in the matrix smaller. This leads to a decrease in the number of wavefunctions $\varphi_\nu^{(i)}$ of localized states in the CES (8). Thus, inelastic resonance electron tunnelling via a chain of localized states in the matrix is depressed. This reduces the transparency of the tunnelling barrier in (10), and the coefficient η grows. Therefore, the CES localization size L and the imaginary part of the dielectric constant ε'' decrease.

Experimental frequency dependences of ε'' exhibit a decrease in their values with increasing frequency. This fact can be explained in terms of the theoretical CES model we developed. The imaginary part of the dielectric constant in equation (13) decreases in accordance with the function $\varepsilon'' \propto \omega^{-1}$.

The nature of the maximum in ε'' for granular films deposited onto cold substrates in the Ar + O_2 plasma at metal concentration $x = 55$ at.% (figure 3(b)) is unclear. This maximum correlates with the maximum in μ'' and may be a consequence of a correlation between the spin directions of neighbouring granules. In this case, the granular films are in the ferromagnetic state at $x > 55$ at.%. The appearance of a ferromagnetic domain structure may reduce the CES localization size. This hypothesis requires additional experimental and theoretical verification.

5. Conclusion

We have investigated dielectric and magnetic losses of microwave electromagnetic radiation in granular structures with ferromagnetic nanoparticles $(\text{a-SiO}_2)_{100-x}(\text{Co}_{0.4}\text{Fe}_{0.4}\text{B}_{0.2})_x$ and obtained the following results.

(1) For granular structures prepared in the Ar + O_2 plasma with granule concentrations below the percolation region, the decay constant of the granule spin relaxation grows with decreasing metal content. This phenomenon is accounted for by the SPR occurring

via simultaneous changes in the granule spin direction and in the spin polarization of electrons on exchange-split localized states at impurity and defects sites in the matrix. These localized states have exchange splitting energies equal to microwave energies and lie at a greater distance from the ferromagnetic granules compared with the radius of the exchange interaction. With increasing granule concentration, these energy-exchange splittings are broadened by neighbouring granules and give no contribution to the SPR. This leads to a decrease in the number of magnetically active matrix levels per granule with increasing metal content and gives the observed decay dependences.

(2) As-sputtered granular films prepared in argon show lower magnetic losses than films deposited in the $Ar + O_2$ atmosphere. This is due to different structures of localized electron states of impurities in the matrix, which are formed by reactive gases. Argon atoms form impurities with filled exchange-split levels, which are not polarized and take no part in the SPR. Annealing removes some electrons from the filled levels and Ar impurities become spin polarizable, which makes the magnetic losses higher. Oxygen atoms form in the matrix impurities with partially filled exchange-split levels. They are magnetically active, can be polarized and take part in the SPR. Annealing partly reduces the amount of the oxygen impurities.

(3) At microwave frequencies we have observed a sharp increase in dielectric losses with increasing metal content in the percolation region and different dielectric losses for structures sputtered in the Ar plasma and in the $Ar + O_2$ atmosphere. Annealing reduces the imaginary part of the dielectric constant. The observed behaviour of dielectric losses can be explained in terms of the model of dielectric constant, based on CESs. This behaviour is due to electric dipole polarization of electrons in CESs formed by s-electrons of granules near the Fermi level and by electrons of matrix localized states in the intergranule regions. The imaginary part of the dielectric constant is proportional to the CES localization size. In the percolation region, the characteristic CES localization size becomes infinite, which leads to a sharp increase in dielectric losses. Annealing reduces the number of localized electron states in the matrix and makes the CES size smaller. The theoretical model of CESs we have developed takes into account the randomness of the granule size. To develop a more exact model, we should take into consideration the randomness of the tunnelling coefficient between granules and use more exact CES wavefunctions. However, despite this, the above simple model of the dielectric constant, based on CESs, accounts adequately for the experimental dependences and can be regarded as a step towards developing a quantum theoretical model of percolation in granular structures.

Acknowledgment

Authors wish to thank P G Lederer for helpful discussions.

References

[1] Wang Wen-Nai, Jiang Zheng-Sheng and Du You-Wei 1995 *J. Appl. Phys.* **78** 6679
[2] Butera A, Zhou J N and Barnard J A 1999 *Phys. Rev.* B **60** 12270
[3] Butera A, Zhou J N and Barnard J A 2000 *J. Appl. Phys.* **87** 5627
[4] Morikawa T, Suzuki M and Taga Y 1998 *J. Appl. Phys.* **83** 6664
[5] Ohnuma S, Kobayashi N, Masumoto T, Mitani S and Fujimori H 1999 *J. Appl. Phys.* **85** 4574
[6] Lutsev L V 2002 *Phys. Solid State* **44** 102
[7] Siklitskii V I, Lutsev L V and Baidakova M V 2002 *Tech. Phys. Lett.* **28** 283
[8] Bunde A, Coniglio A, Hong D C and Stanley H E 1985 *J. Phys. A: Math. Gen.* **18** L137

[9] Hong D C, Stanley H E, Coniglio A and Bunde A 1986 *Phys. Rev.* B **33** 4564
[10] Kalinin Yu E, Ponomarenko A T, Sitnikoff A V and Stognei O V 2002 *Proc. 18th Int. School-Workshop 'Novel Magnetic Materials for Microelectronics' (Moscow 2002)* p 575
[11] Zolotukhin I V, Kalinin Yu E, Sitnikoff A V and Stognei O V 2002 *Proc. 18th Int. School-Workshop 'Novel Magnetic Materials for Microelectronics' (Moscow 2002)* p 655
[12] Sankar S, Dender D, Borchers J A, Smith D J, Erwin R W, Kline S R and Berkowitz A E 2000 *J. Magn. Magn. Mater.* **221** 1
[13] Izyumov Yu A, Kassan-ogly F A and Skryabin Yu N 1974 *Field Methods in Theory of Ferromagnetism* (Moscow: Nauka) (in Russian)
[14] Shklovskii B I and Efros A L 1984 *Electronic Properties of Doped Semiconductors* (New York: Springer)
[15] Landau L D and Lifshitz E M 1982 *Electrodynamics of Continuous Media* (Moscow: Nauka) (in Russian)
[16] Lutsev L V, Yakovlev S V and Siklitskii V I 2000 *Phys. Solid State* **42** 1139
[17] Mott N F and Davis E A 1979 *Electron Processes in Non-Crystalline Materials* (Oxford: Clarendon)
[18] Glazman L I and Shekhter R I 1988 *Sov. Phys.–JETP* **67** 163
[19] Glazman L I and Matveev K A 1988 *Sov. Phys.–JETP* **67** 1276
[20] Lutsev L V, Kalinin Yu E, Sitnikoff A V and Stognei O V 2002 *Phys. Solid State* **44** 1889
[21] Kraeft W-D, Kremp D, Ebeling W and Röpke G 1986 *Quantum Statistics of Charged Particle Systems* (Berlin: Akademie-Verlag)